Eur. Phys. J. D **15**, 293–300 (2001)

THE EUROPEAN PHYSICAL JOURNAL D

EDP Sciences

Experimental study and Monte Carlo simulation of the correlation between electron emission and stopping power for swift proton impact on amorphous carbon target

M. Beuve[1], M. Caron[1,a], B. Gervais[1], H. Rothard[1,b], A. Clouvas[2], and C. Potiriadis[3]

[1] Centre Interdisciplinaire de Recherche Ions Lasers CIRIL (CEA-CNRS-ISMRA), B.P. 5133, rue Claude Bloch, 14070 Caen Cedex 05, France
[2] Department of Electrical and Computer Engineering, Aristotle University of Thessaloniki, 54006 Thessaloniki, Greece
[3] Greek Atomic Energy Commission, 15310 Agia Paraskevi, Greece

Received 9 March 2001

Abstract. It is usually well accepted that for swift protons, the induced backward and forward electron emission yield is proportional to the projectile electronic stopping power. This was observed in particular for thin amorphous carbon foils. However, this law was established from a non extensive set of experimental data and somewhat confirmed by rough macroscopic theories. We then developed a standard Monte Carlo simulation to predict the yield dependence on proton energy [0.5–10 MeV] and for a wide range of foil thickness. After evaluating the reliability of this simulation, we showed and explained why the law of proportionality cannot generally hold for forward electron emission. In particular, the ratio between forward yield and stopping power generally depends on foil thickness and proton energy. We performed a new experiment that confirmed our theoretical predictions.

PACS. 34.50.Bw Energy loss and stopping power – 79.20.Ap Theory of impact phenomena; numerical simulation – 79.20.Rf Atomic, molecular, and ion beam impact and interactions with surfaces

1 Introduction

Secondary electron emission induced by the penetration of swift charged particles in a solid has been of interest for a long time. Electron emission from solid surfaces was first observed over 100 years ago [1–5] and during the last 30 years was extensively analysed through all available experimental parameters (projectile atomic number and energy, incident projectile charge state, target atomic number and thickness, angle of incidence, etc.). Important applications concern track formation in solids, detectors of heavy ions and tumour treatment by heavy ion beams just to name a few. Extensive reviews on electron emission from solids can be found in references [6–9].

The knowledge of the mean number of electrons emitted per incoming projectile (the electron yield γ) as well as their angular and energy distribution is of fundamental interest. In case of sufficiently thin foils, electrons are ejected from both the entrance and exit surface of the solid (*cf.* Fig. 1) and it is possible to decompose the above mentioned electron yield γ in forward (emission in the direction of the projectile beam) and backward (emission in the direction opposite to the projectile beam) contributions, γ_F and γ_B, respectively. Both γ_F and γ_B were found to be proportional to the electronic energy loss per unit path length (stopping power) dE/dx for proton impact on carbon as a function of projectile velocity over a wide range of velocities [10]. Nevertheless this study was performed only for a target thickness of 16 $\mu g/cm^2$.

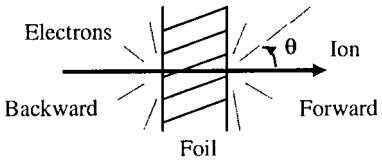

Fig. 1. Schematic representation of the beam foil interaction. Note that the backward hemisphere corresponds to the entrance surface for the ion.

The correlation between electron emission and stopping power is also assumed in some existing theoretical models, which, despite the complex problem that electron emission represents, were developed rather soon after the first experimental studies [11]. However, the approaches were very phenomenological and macroscopic [12–15] and the relation between the system parameters and the electron emission quantities implied the adjunction of a wide range of assumptions [16,17]. In particular, most of these

[a] *Present address*: PHILIPS GmbH, Philips Research Laboratories, Nanomaterials D303, Weisshausstrasse 2, 52066 Aachen, Germany.
[b] e-mail: `rothard@ganil.fr`

models assume an isotropic distribution of ejected electrons and for this reason they cannot distinguish between forward and backward electron emission. To date, one of the most successful empirical models that deals with backward and forward emission was proposed by Koschar *et al.* [18]. It explicitly takes into account the production of fast δ-electrons in the forward direction, which is at the origin of the backward/forward asymmetry in electron emission. Nevertheless we shall see later that this model does not predict the correct relationship between the yield and the stopping power, in particular for large foil thickness.

Monte Carlo simulation [8,19–24] is a powerful tool to study ion induced electron emission. In contrast to macroscopic models, Monte Carlo (MC) simulation does not make the assumption of a primary spectrum proportional to stopping power. Indeed, primary collisions of the projectile with the target electrons, as well as all the collisions that the electron emission process implies, are treated from a microscopic point of view within quantum formalism. For protons, such a MC simulation leads to a proportionality between γ_{B} and $\mathrm{d}E/\mathrm{d}x$ for a thick carbon target [25]. However, it is interesting to note that the same authors observed a slightly different behaviour for thick aluminium target.

In the present work, the correlation between electron emission and stopping power for proton impact (0.5–10 MeV) on thin carbon foils of different thickness (1–1025 $\mu\mathrm{g/cm}^2$) is studied theoretically (by MC simulation) and experimentally. The theoretical aspects will be presented in Section 2.1 and thoroughly discussed in Sections 2.2 and 2.3. A complete set of experimental data will be presented and discussed in the light of theoretical results in Section 3.

2 Theoretical analysis

2.1 Monte Carlo simulation of electron emission

Following numerous authors in this field [6,22,26], we describe our system with the help of a phenomenological master equation we can derive under the following assumptions. We consider the electron emission as a two-step phenomenon. First the interaction between the projectile ion and the target liberates electrons above the Fermi energy of the target and then the excited electrons diffuse in a potential that represents the solid. During their diffusion the excited electrons can liberate other target electrons giving rise to a cascade phenomenon. The interaction with the surface is taken into account by considering that the electrons move in the target potential [23,24]. We assume that electron transport results from a series of stochastic collisions, and that it can be described classically on a mesoscopic scale (*i.e.* its position $\mathbf{r}$ and momentum $\mathbf{p}$ are simultaneously well defined), whereas the collisions follow quantum mechanical rules. Since the protons are quite fast (say, with kinetic energy above 0.1 MeV) they can be assumed to propagate along an unperturbed straight line with a constant velocity and a constant charge Q_{P} equal to 1. The master phase space equation reads:

$$\frac{\partial f}{\partial t} + \mathbf{p}\cdot\boldsymbol{\nabla}_{\mathbf{r}} f - \boldsymbol{\nabla}_{\mathbf{r}} V_0 \cdot \boldsymbol{\nabla}_{\mathbf{p}} f + k(\mathbf{p}) f - \int \mathrm{d}\mathbf{p}'\, K(\mathbf{p},\mathbf{p}') f(\mathbf{p}') = S(\mathbf{p}) \quad (1)$$

where $f(\mathbf{r},\mathbf{p},t)$ is the number of excited electrons at the phase space coordinate ($\mathbf{r}$, $\mathbf{p}$) at time t. $k(\mathbf{p})$ is the probability per unit of time that an electron changes its momentum $\mathbf{p}$ due to collisions. $K(\mathbf{p},\mathbf{p}')$ is the probability per unit of time that from such a collision (of an electron with initial momentum $\mathbf{p}'$) either a secondary electron with momentum $\mathbf{p}$ is created, or that the primary electron changes its momentum to $\mathbf{p}$ by deflection and energy loss. $S(\mathbf{p})$ is the number of electrons liberated per unit of time with a momentum $\mathbf{p}$ by the projectile. From the distribution function f we obtain γ_{F} and γ_{B} as follows:

$$\gamma_{\mathrm{F,B}} = \lim_{t\to+\infty} \int_{\mathrm{B,F}} \mathrm{d}\mathbf{r} \int \mathrm{d}\mathbf{p}\, f(\mathbf{r},\mathbf{p},t). \quad (2)$$

Note that the left-hand side of equation (1) is linear with respect to f. This means that the scaling properties of $S(\mathbf{p})$ will produce the same scaling properties for the yields. Obviously, the scaling properties of $S(\mathbf{p})$ apply to the stopping power as well and if we could find two ions for which $S_1(\mathbf{p}) = \alpha S_2(\mathbf{p})$, the yield would follow the stopping power. Such a kind of scaling may be found for two fast light ions at the same velocity in a limited range of charge [27]. This is however not the case when the projectile velocity v_{P} is changed. Indeed, a change in v_{P} induces changes in the kinematics of ion-electron collisions, which results in a deformation of $S(\mathbf{p})$. We emphasise that $S(\mathbf{p})$ is not isotropic as it can be observed in Figure 2, where we have plotted for a given foil thickness, the energy differential primary spectra emitted in 3 different directions, for two different ion velocities (0.5 MeV and 9.2 MeV). For comparison, each spectrum is normalised to the corresponding electronic stopping power. The jitter comes from the statistics of the Monte Carlo simulation. Note the strong resemblance of both backward spectra and the qualitative difference in the high-energy part of both forward spectra. Therefore, the proportionality between γ, γ_{B} or γ_{F} with the stopping power has only two possible interpretations:

1. the linear master equation (1) is wrong despite its great success in explaining many results about electron emission [21–24,26];
2. the transport properties of the kernel in equation (1) permits, by chance, that the solution of equation (1) predicts an approximate proportionality either for γ_{B} or γ_{F}.

The second interpretation was qualitatively discussed before [17], and we shall examine it more closely in the next section for the condition of the experiment performed so far.

The master equation (1) may be handled in several ways. A well-suited choice is a standard Monte Carlo

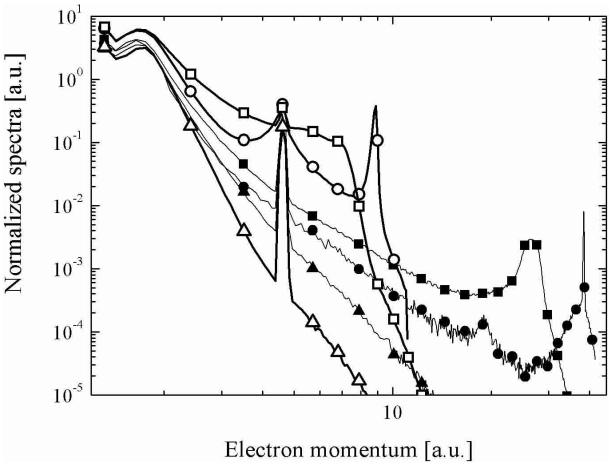

Fig. 2. Momentum and solid angle spectra of primary electrons calculated for 0.5 MeV protons (open symbol) and 9.2 MeV protons (full symbol) with a thickness of 1 μg/cm^2. Each spectrum is normalized to the corresponding proton stopping power. Angles: 3° (circle), 45° (square) and 135° (triangle). Channel widths: $\Delta p = 0.11$ a.u.; $\Delta\theta = \pm 0.025$ rad (for 9.2 MeV protons) and $\Delta\theta = \pm 0.015$ rad (for 0.5 MeV protons).

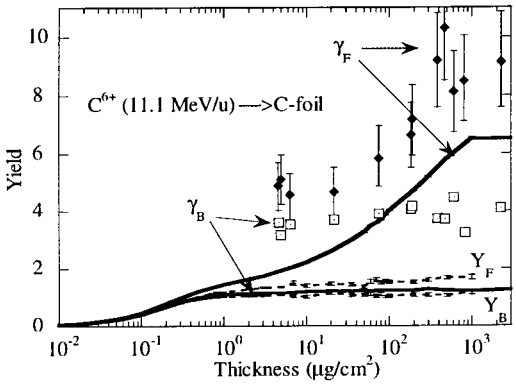

Fig. 3. Backward γ_B and forward γ_F yield evolution with foil thickness. Experimental data of Jung *et al.* [34] (symbols). Present theory (solid line). Low-energy electron contribution to the yields, calculated for backward Y_B and forward Y_F emission (dotted line).

(MC) simulation [24,28] that does not require any further assumptions. In the simulation the particles are followed from the entrance of the ion in the solid until the electrons leave the solid or until their energy becomes so small that they cannot exit the solid potential anymore (*i.e.* they have a negative energy with respect to vacuum level). The position of the Fermi level is obtained from the work function of graphite taken at 0.173 a.u. (4.7 eV) below the vacuum level [29]. The potential inside the target is taken to be $V_0 = -0.895$ a.u. (-24.3 eV). It corresponds to the bottom of the conduction band for a uniform gas of independent electrons at the same density ($4\rho_{At}$), which is usually chosen [21–24,26,30]. Note that the absolute value of the yield is highly sensitive to the choice of V_0 [23,24]. The kernel entering equation (1) includes elastic scattering on target nuclei as well as inelastic scattering and ionisation by collision with the valence and $1s$ core electron. For this latter interaction, Auger electron emission is accounted for. More details about the kernel can be found elsewhere [21–24,26,31].

In the calculation presented in this paper, the proton interaction with the valence electrons is described in the framework of dielectric response theory, while the $1s$ target electron ionisation is modelled by the CDW-EIS theory. A more thorough description is not necessary for our purpose and we refer the interested reader to the following references [24,32].

2.2 Analysis of transport effects

Although nowadays the main transport effects are well-known from experimental data [33–35], macroscopic models [14,18] and more sophisticated models [23,24], we shall move one step back and re-analyse the evolution of the yield with the foil thickness. The purpose of this section is, first, to check the reliability of our Monte Carlo code by comparing it to experimental data, second, to call to mind some transport effects relevant for the relation between electron emission and stopping power, and third, to shed some new light on this subject. Figure 3 presents the theoretical predictions for γ_B and γ_F for 11.1 MeV/u C^{6+} as a function of the foil thickness. It also displays the contribution of the low-energy electrons to the yields (*i.e.* energy lower than 50 eV in vacuum). The error bars on the MC curves indicate the small statistical dispersion. From the figure, most of the backward ejected electrons are low-energy electrons. As a consequence, γ_B keeps increasing with foil thickness until this thickness becomes larger than the escape length, *i.e.* the maximal depth for the low-energy electrons to be able to escape the solid. From the yield-thickness curve we obtain for this escape length about 50 a.u. (2.5 nm), in reasonable agreement with the literature [18,37].

The evolution of γ_F with the foil thickness is notably different from the evolution of γ_B. Indeed, even if γ_F essentially matches its backward counterpart for thickness lower than the low-energy electron escape length, γ_F keeps increasing for thicker foils. The reason for this increase are the anisotropy of the source term previously mentioned in Section 2.1 and the ejection of fast electrons in the forward direction. Though the total probability of fast electron ejection is quite low, it is not negligible in the forward direction and these fast electrons can easily escape from the foil (*cf.* Tab. 1) compared to low-energy electrons. Therefore, when further increasing the foil thickness, fast electrons from deeper layers can still escape from the foil. They are thus cumulated, increasing the number of electrons ejected in the forward direction. Finally, when the thickness exceeds the maximum escape length for the fastest electrons (*cf.* Tab. 1), γ_F reaches a saturation value. The deduced saturation thickness corresponds to the penetration depth of electrons [31] whose velocity is two times that of the projectile, *i.e.* the fastest electrons emitted by the projectile. Let us note that the low-energy electron contribution to γ_F at the saturation thickness is close to

Table 1. Estimation of the velocity ($V_{max} = 2V_p$), the energy ($E_{max} = 2V_p^2$) and the range (R_m [31]) of the fastest primary electrons for various proton energies (E_p).

E_p (MeV)	V_{max} (a.u.)	E_{max} (keV)	R_m (μg/cm^2)
0.5	8.96	1.09	6.66
1	12.66	2.18	21.49
2	17.91	4.36	69.35
3	21.93	6.54	137.62
4	25.32	8.72	223.78
5	28.31	10.90	326.28
6	31.02	13.08	444.03
7	33.50	15.26	576.17
8	35.81	17.44	722.03
9	37.99	19.62	881.06
10	40.04	21.80	1052.77

that of the backward yield. In other words, the difference between backward yield and forward yield mostly consists in cumulated fast electrons. This means also that the slowing down of the fast electrons results in the production of very low-energy electrons that cannot escape the foil. This is somewhat in contradiction to assumptions of the macroscopic models, in which it is assumed that most of the emitted electrons originate from a large cascade multiplication instead of being primaries [17,18].

Figure 3 also provides a comparison to the experimental data of Jung *et al.* [34,37]. We observe a rather good agreement in shape between the experiment and our theory. Nevertheless, we note a discrepancy in absolute value. It is very likely due to an incorrect description of low-energy electron transport, which underestimates the low-energy electron contribution to the yields. It could also be due to some extent to an overestimation of the experimental values obtained in standard vacuum with uncleaned target instead of ultra high vacuum. It is, however, the evolution with target thickness which is important in the present context.

Figure 4 shows the influence of the projectile velocity on the yield evolution versus thickness for 0.5 MeV/u and a 9.2 MeV/u H^+. Obviously, the yields for the slower proton are higher than for the faster proton. Except for this difference in absolute value, the behaviour of the backward yield is similar at both velocities. We also calculated the stopping power fraction that corresponds to the ejection of fast primary electrons (larger than 50 eV with respect to the vacuum level). We obtained 58.6% for the 0.5 MeV/u H^+ and 63.3% for the 9.2 MeV/u H^+. Since these values are rather close, one would expect a similar evolution of forward yield with the thickness for both velocities. In contrast, two striking differences are observed. First, the saturation thickness is much lower for the slowest proton. In fact, the saturation thickness corresponds to the penetration depth of electrons whose velocity is twice the projectile velocity (*i.e.* 7 μg/cm^2 at 0.5 MeV and 900 μg/cm^2 at 9.2 MeV, *cf.* Tab. 1 and Fig. 4). Second, the ratio between γ_F and γ_B at saturation is about two times higher for the faster proton than for the slower. This means that for high proton velocity, the few additional faster electrons from deeper layers contribute significantly and strongly increase γ_F, though their contribution to the energy loss is small. In other words, matter acts as a high-pass filter that allows only for high-energy electron transmission. Consequently, γ_F *cannot be possibly simply related to stopping power*, as pointed out in Section 2.1. The proportionality between γ_F and stopping power observed by Clouvas *et al.* [10] (*cf.* Fig. 5a) is therefore astonishing and led us to re-analyse the experimental data and to perform a new experiment.

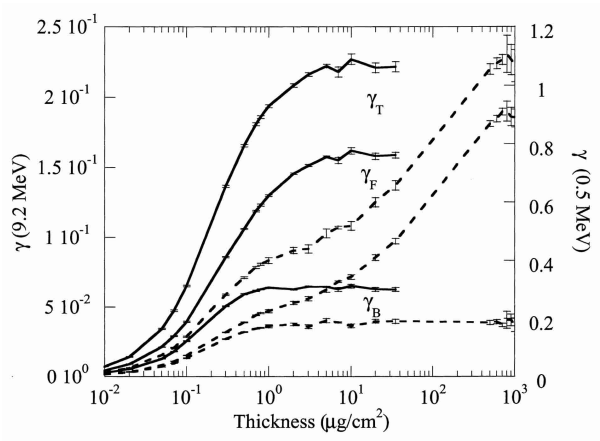

Fig. 4. Backward γ_B and forward γ_F yield evolution with foil thickness, calculated for a 0.5 MeV proton (solid line) and a 9.2 MeV proton (dashed line).

2.3 Calculated thickness dependent electron yields

We have calculated the ratio Λ of the yield over stopping power with the following thickness:

(i) a thickness of 16 μg/cm^2, which corresponds to the foil thickness used by Clouvas *et al.* [10];
(ii) a thickness of 1 μg/cm^2, which represents the regime for which the cascades of fast electrons remain negligible;
(iii) the saturation thickness, which depends on the energy of the projectile and which integrates the whole development of the fast electron cascades.

The results are presented in Figure 5b.

We first observe that, within the error bars, the ratio for backward emission Λ_B is independent of the projectile energy and of the target thickness as expected for γ_B. It saturates for thickness higher than 1 μg/cm^2. The independence with projectile energy can be explained in the following way. From the simulation, we know that the backward yield mostly consists in slow secondary electrons induced by slow primaries. This particular contribution to γ_B is observed to be proportional to the energy lost by the projectile to generate slow primary electrons in the typical escape depth of slow electrons [23,25,38]. Moreover, the relative fraction of energy lost in slow primary creation is only weakly dependent on the projectile velocity (36% at 0.5 MeV and 29% at 9.0 MeV). In absolute value, it is thus

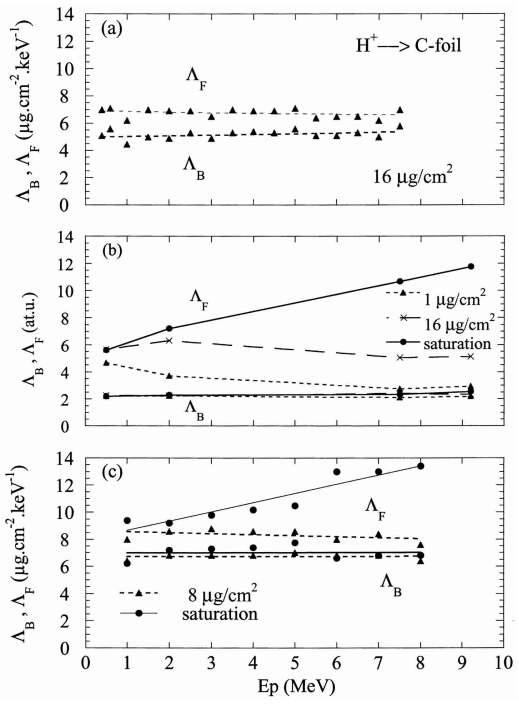

Fig. 5. Ratio of yields and stopping power, for forward Λ_F and backward Λ_B emission, as a function of the proton energy. (a) Experimental data obtained with a thickness of 16 μg/cm^2 [10]. (b) Our theoretical predictions obtained for thickness of 1 and 16 μg/cm^2 and for the saturation thickness. (c) Our experimental data obtained for a thickness of 8 μg/cm^2 and for the saturation thickness.

roughly proportional to the stopping power. This proportionality is an excellent approximation for an amorphous carbon target. We confirm here the results obtained by Dubus *et al.* in the energy range 0.25−3.0 MeV for aluminium [25].

Second, we observe that the ratio for forward emission Λ_F dramatically depends both on the projectile energy and on the foil thickness. While this ratio increases with the projectile energy for the saturation thickness, it decreases for the thickness of 1 μg/cm^2. At low thickness, the fast protons lose energy to generate fast electrons, which contribute few to the forward yield, and Λ_F is then low. In contrast, at saturation thickness all the target layers contributes and the electron emission is maximum. Finally, for 1 μg/cm^2, Λ_F is clearly higher for 0.5 MeV/u H^+ than for 9.2 MeV/u H^+ while at saturation thickness the opposite trend is observed. Indeed, high-pass energy filtering of matter leads to Λ_F much higher for fast proton than for slow proton. The thickness of 16 μg/cm^2 is an intermediate thickness and, fortuitously, Λ_F seems constant within ±10%. The macroscopic model proposed by Koschar *et al.* [18] qualitatively includes some of these important effects and due to its free parameters its predictions can match some experimental data. However the assumed laws are quantitatively not relevant enough to provide a correct description for γ_F. In particular, in contradiction with our simulation, γ_F is found to be proportional to the stopping power for large thickness.

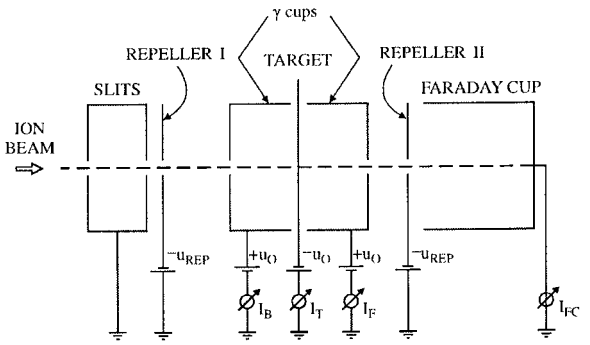

Fig. 6. Schematic experimental setup.

To summarise, from our simulation we confirm the proportional relation between backward yield and stopping power for 0.5 MeV–9.2 MeV/u protons and for carbon foil thickness larger than 1 μg/cm^2. On the other hand, such a relation for forward emission cannot be generally expected, and the experimental results obtained by Clouvas *et al.* [10] were obtained for a target thickness at which the velocity dependence of Λ_F is quite small. Guided by the above theoretical results, we performed a new experiment of target thickness and energy dependent proton induced electron yields.

3 Experimental procedure and results

The experimental work was performed at the 5 MV Tandem accelerator of the National Research Center of Physical Sciences "Demokritos" in Athens, Greece. Mass analysed beams of protons (1–8 MeV) were sent through thin (8–1025 μg/cm^2) self-supporting carbon foils.

The experimental set-up used for these measurements is shown in Figure 6. Two nearly closed metal cylinders (similar to Faraday cages, except for openings for the incoming and outgoing ion beam) mounted on each side of a target-foil holder were used to collect the secondary electrons in the forward and the backward directions of the target foil simultaneously, but separately. The cylinders were held at a potential $+U_0 = +40$ V to assure that all the secondary electrons were collected, and a negative potential of $-U_0 = -20$ V was applied to the target, enough for the electron emission γ to reach the saturation value. The Faraday cup was comprised of two parts: a beam collecting cup that was grounded through an electrometer and a cylindrical electrode upstream of this cup which was biased $-U_0 = -300$ V relative to the ground. This negatively biased electrode prevented (i) secondary electrons of the target from escaping from the collecting cup and (ii) secondary electrons of the target from escaping through the opening of the outgoing ion beam of the second cylinder (γ cup). A similar repeller (Repeller I) was positioned upstream of the first γ-cup and biased $-U_{rep} = -300$ V with respect to the ground in order to prevent (i) secondary electrons from the slits to hit the

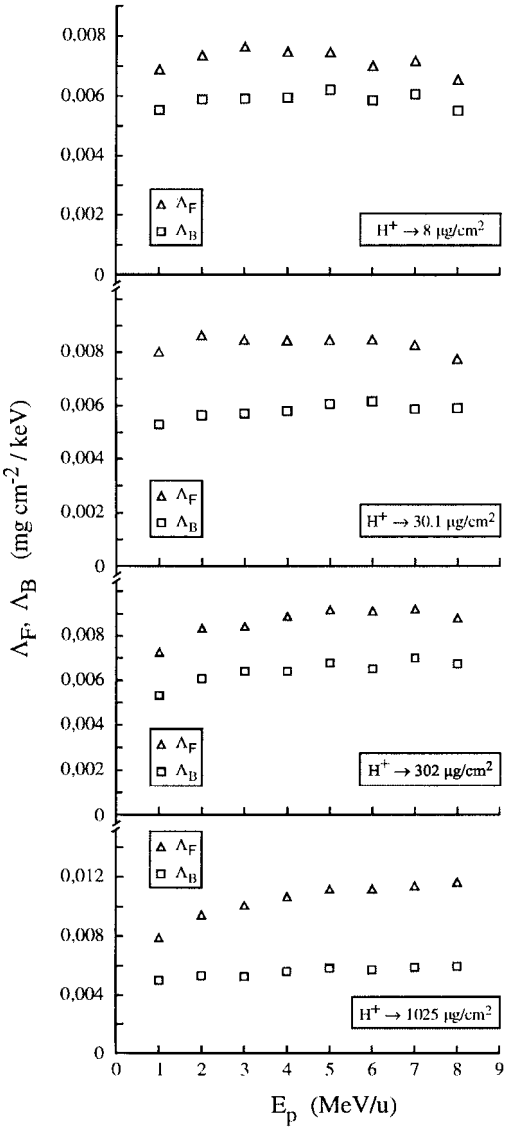

Fig. 7. Energy dependence of the Λ_B, Λ_F for proton ions impinging on carbon foils. Λ_F is calculated with the stopping power at the exit of the foil.

first γ cup and (ii) secondary electrons of the target from escaping through the opening of the incoming ion beam of the first γ cup. The experiments were performed under standard vacuum conditions (10^{-4}–10^{-5} Pa).

Backward (γ_B), forward (γ_F), and total (γ_T) electron yields can easily be deduced from measuring: the ion induced target current I_T, the current of low energy electrons I_B and I_F, and the ion beam current I_{FC}:

$$\gamma_B = \frac{I_B}{I_{FC}}, \quad (3)$$

$$\gamma_F = \frac{I_F}{I_{FC}}, \quad (4)$$

$$\gamma_T = \frac{I_T}{I_{FC}} \cdot \quad (5)$$

Table 2. Estimation of the mean energy of outgoing protons (in MeV) as a function of the foil thickness and of the energy of the incoming protons [39].

	Thickness (μg/cm^2)			
	30	90	302	1025
E_p (MeV)				
1	0.99	0.98	0.93	0.74
2		1.99	1.96	1.85
3			2.97	2.88
4			3.97	3.91
5			4.98	4.92
6			5.98	5.93
7				6.94
8				7.95
9				8.95
10				9.96

Table 3. Estimation of the stopping power (in MeV/(mg/cm^2)) for outgoing protons as a function of the foil thickness and of the energy of the incoming protons [39].

	Thickness (μg/cm^2)				
	0	30	90	302	1025
E_p (MeV)					
1	0.229	0.230	0.232	0.240	0.276
2	0.143		0.144	0.146	0.152
3	0.107			0.108	0.111
4	0.0860			0.0865	0.0877
5	0.0723			0.0726	0.0733
6	0.0626			0.0628	0.0632
7	0.0553				
8	0.0497				
9	0.0451				
10	0.0414				

The γ_F, γ_B, γ_T for four different targets with thickness 8, 30, 302, 1025 μg/cm^2 are measured at different proton energies (1–8 MeV). The results are shown in Table 4. The errors of all coefficients are estimated to be 5% (based on reproducibility measurements). For all ions we observe that within 2% $\gamma_T = \gamma_F + \gamma_B$. This means that the fraction of forward emitted high energy delta electrons, which can escape through the opening of the outgoing ion beam of the second cylinder (γ cup), is small.

The ratios Λ_F, Λ_B are calculated using the stopping powers (dE/dx) obtained from the TRIM code [39], which gives electronic stopping power values in agreement with other recent values [40].

The experimental ratios are presented in Figure 5c: (i) for the thinnest foil (8 μg/cm^2); (ii) for foils chosen so that, for each proton energy, the thickness is as close as possible to the estimated saturation thickness (*cf.* Tab. 1). We observe that the evolution of the ratios with the thickness is in really good agreement with the prediction (*cf.* Fig. 5b). For backward emission, the ratio is clearly constant. For forward emission, the ratio is increasing for the saturation thickness and decreasing for the thin foil, demonstrating experimentally that the forward yield is not at all proportional to the stopping power. The trends

Table 4. For various energies of incoming protons and various foil thickness: experimental values for total (γ_T), backward (γ_B) and forward (γ_F) yields; estimation of the stopping power for incoming and outgoing protons [39] in keV/(mg/cm^2). Thickness: 8 μg/cm^2 (a), 30.1 μg/cm^2 (b), 302 μg/cm^2 (c), 1025 μg/cm^2 (d).

(a)

E_p (MeV)	γ_T	γ_B	γ_F	dE/dx (inc.)	dE/dx (out.)	Λ_B	Λ_F
1	2.93	1.27	1.58	229.5	229.8	0.00553	0.00687
2	1.92	0.83	1.04	141.2	141.2	0.00588	0.00736
3	1.45	0.62	0.8	104.7	104.7	0.00592	0.00764
4	1.17	0.5	0.63	84.1	84.11	0.00594	0.00749
5	1	0.44	0.53	70.8	70.80	0.00621	0.00748
6	0.83	0.36	0.43	61.4	61.41	0.00586	0.00700
7	0.74	0.33	0.39	54.3	54.30	0.00608	0.00718
8	0.62	0.27	0.32	48.9	48.9	0.00552	0.00654

(b)

E_p (MeV)	γ_T	γ_B	γ_F	dE/dx (inc.)	dE/dx (out.)	Λ_B	Λ_F
1	3.17	1.22	1.85	229.5	230.4	0.00532	0.00803
2	2.05	0.8	1.22	141.2	141.4	0.00567	0.00862
3	1.52	0.6	0.89	104.7	104.7	0.00573	0.00849
4	1.23	0.49	0.71	84.1	84.13	0.00583	0.00844
5	1.06	0.43	0.6	70.8	70.81	0.00607	0.00847
6	0.93	0.38	0.52	61.4	61.41	0.00619	0.00847
7	0.78	0.32	0.45	54.3	54.30	0.00589	0.00829
8	0.7	0.29	0.38	48.9	48.90	0.00593	0.00777

(c)

E_p (MeV)	γ_T	γ_B	γ_F	dE/dx (inc.)	dE/dx (out.)	Λ_B	Λ_F
1	3.15	1.22	1.76	229.5	242.0	0.00532	0.00727
2	2.09	0.86	1.2	141.2	143.7	0.00609	0.00835
3	1.59	0.67	0.89	104.7	105.5	0.00640	0.00843
4	1.32	0.54	0.75	84.1	84.50	0.00642	0.00888
5	1.16	0.48	0.65	70.8	70.99	0.00678	0.00915
6	1	0.4	0.56	61.4	61.50	0.00651	0.00910
7	0.9	0.38	0.5	54.3	54.35	0.00700	0.00920
8	0.77	0.33	0.43	48.9	48.92	0.00675	0.00879

(d)

E_p (MeV)	γ_T	γ_B	γ_F	dE/dx (inc.)	dE/dx (out.)	Λ_B	Λ_F
1	3.47	1.15	2.24	229.5	283.9	0.00501	0.00789
2	2.21	0.75	1.42	141.2	150.3	0.00531	0.00944
3	1.67	0.55	1.09	104.7	107.8	0.00525	0.0101
4	1.4	0.47	0.91	84.1	85.49	0.00559	0.0106
5	1.24	0.41	0.8	70.8	71.48	0.00579	0.0112
6	1.08	0.35	0.69	61.4	61.74	0.00570	0.0113
7	0.97	0.32	0.62	54.3	54.47	0.00589	0.0114
8	0.88	0.29	0.57	48.9	48.97	0.00593	0.0116

are however less obvious than the ones predicted by the theory, likely because the low-energy electron contribution is higher than the predicted one. Moreover, the thinnest foil is 8 μg/cm^2 for the experiment and 1 μg/cm^2 for the theory.

Figure 7 brings another point of view for these features. Instead of considering the saturation thickness, the forward and backward ratios are simply plotted as a function of projectile energy for the whole set of experimental thickness. Now, the forward ratio is no longer calculated with the stopping power at the "entrance" but with the stopping power at the "exit" of the foil. Indeed, as exemplified by Tables 2 and 3, the slowest protons lose velocity and their stopping power actually increases. Once more, we observe, in particular for the thickest foil, that the forward yield is not simply proportional to stopping power.

4 Conclusion

Focusing on 0.5–9.2 MeV/u protons and on an amorphous carbon target, we have re-analysed, in the light of a Monte Carlo simulation, the relation between proton induced electron emission yields and proton stopping power. We show that, due to a transport effect, no simple relation could be expected for forward emission. In

fact, forward yields depend on the spectra in energy and angle of the primary electrons, on one hand, and on the target parameters that characterise electron transport, on the other hand. Although some of these effects are qualitatively included in the macroscopic model proposed by Koschar *et al.* [18], the rough assumptions prevent it from correct predictions, in particular for large thickness. We evaluated the reliability of our simulation through a comparison with experimental data of yield evolution with foil thickness, and predicted the ratios of yields and stopping power. We confirmed and explained the proportionality between backward yield and stopping power. We also confirmed the experimentally observed proportionality for forward yields in the specific range of foil thickness used in previous experiments. However, Λ_F generally depends on the target thickness and on proton energy and it cannot be considered as a material parameter even for protons. The new experimental data that we obtained for a set of amorphous carbon foil thicknesses confirmed nicely the theoretical predictions. The main reason for this behaviour of Λ_F is that the forward electron emission is made of fast electrons coming from deep layers, which add to each other until the saturation thickness is reached. This theoretical result could easily be checked experimentally to establish it definitely.

Beyond the field of proton induced electron emission, this work is of interest for heavier projectiles. Indeed it had been mentioned that for swift heavy ions the lack of the proportionality relation between forward yield and stopping power [37] was likely due to charge effects [34, 35]. This interpretation was proposed from a comparison of experimental data obtained with different foil thickness for protons and for heavy ions. For this reason, we suggest that the effects of transport we considered in this work should play an important role in this comparison. It would be interesting to compare the ratio Λ_F for different atomic number of the projectiles but in the same experimental conditions (nature and thickness of the foils, vacuum conditions). It would allow one to properly establish the respective contributions of high charge effects and of transport effects.

References

1. P.J. Villard, J. Phys. France **8**, 1 (1899).
2. L. Austin, H. Starke, Ann. Physik **9**, 271 (1902).
3. E. Rutherford, Phil. Mag. **56**, 193 (1905).
4. J.J. Thompson, Proc. Cambr. Philos. Soc. **13**, 48 (1906).
5. C. Füchtbauer, Z. Phys. **7**, 153 (1906); C. Füchtbauer, Z. Phys. **7**, 748 (1906).
6. J. Devooght, J.C. Dehaes, A. Dubus, M. Cailler, J.P. Ganachaud, M. Rösler, W. Brauer, in *Particle Induced Electron Emission I*, edited by G. Höhler, E.A. Niekisch, Springer Tracts in Modern Physics (Springer, Berlin, 1991), Vol. 122.
7. D. Hasselkamp, H. Rothard, K.O. Groeneveld, J. Kemmler, P. Varga, H. Winter, in *Particle Induced Electron Emission II*, edited by G. Höhler, E.A. Niekisch, Springer Tracts in Modern Physics (Springer, Berlin, 1991), Vol. 123.
8. M. Cailler, J.P. Ganachaud, Scanning Microsc. Suppl. **4**, 57 (1990); M. Cailler, J.P. Ganachaud, Scanning Microsc. Suppl. **4**, 81 (1990).
9. H. Rothard, Scanning Microsc. **9**, 1 (1995).
10. A. Clouvas, C. Potiriadis, H. Rothard, D. Hofmann, R. Wünsch, K.O. Groeneveld, A. Katsanos, A.C. Xenoulis, Phys. Rev. B **55**, 12086 (1997).
11. H. Frölich, Ann. Phys. (Lpg) **13**, 229 (1932).
12. H. Salow, Z. Phys. **41**, 434 (1940).
13. H. Bruining, *Physics and application of secondary electron emission* (Pergamon, London, 1954).
14. E.J. Sternglass, Phys. Rev. **108**, 1 (1957).
15. R. Baragiola, E.V. Alonso, A. Olivia Florio, Phys. Rev. B **19**, 121 (1979).
16. J. Schou, Phys. Rev. B **22**, 2141 (1980).
17. P. Sigmund, S. Tougaard, Electron emission from solids during ion bombarment, Theoretical aspects, in: *Inelastic Particle-surface collisions*, edited by E. Taglauer, W. Heiland (Springer, Berlin, 1981), p. 2.
18. P. Koschar, K. Kroneberger, A. Clouvas, M. Burhard, W. Meckbach. O. Heil, J. Kemmler, H. Rothard, K.O. Groeneveld, R. Schramm, H.D. Betz, Phys. Rev. A **40**, 2521 (1989).
19. G. Binschas, Z. Phys. **161**, 190 (1961).
20. T. Koshikawa, R. Shimizu, J. Phys. D **7**, 1303 (1974).
21. J.P. Ganachaud, M. Cailler, Surf. Sci. **83**, 488 (1979).
22. A. Dubus, J.C. Dehaes, J.P. Ganachaud, A. Hafni, M. Cailler, Phys. Rev. B **47**, 623 (1993).
23. M. Beuve, thèse de l'université de Caen, 1999.
24. B. Gervais, M. Beuve, in preparation; M. Beuve *et al.*, Phys. Rev. A (submitted, 2001).
25. A. Dubus, M. Rösler, Nucl. Instrum. Meth. Phys. Res. B **115**, 251 (1996).
26. M. Rösler, W. Brauer, Phys. Stat. Sol. (b) **104**, 161 (1981); M. Rösler, W. Brauer, Phys. Stat. Sol. (b) **104**, 575 (1981); M. Rösler, W. Brauer, Phys. Stat. Sol. (b) **148**, 213 (1988).
27. M. Beuve, M. Caron, B. Gervais, H. Rothard, Phys. Rev. B **62**, 8818 (2000).
28. J. Burgdörfer, J. Gibbons, Phys. Rev. A **42**, 1206 (1990).
29. R.F. Willis, B. Fitton, G.S. Painter, Phys. Rev. B **9**, 1926 (1974).
30. M.S. Chung, T.E. Everhart, Phys. Rev. B **15**, 4699 (1974).
31. S. Lencinas, J. Burgdörfer, J. Kemmler, O. Heil, K. Kroneberger, N. Keller, H. Rothard, K.O. Groeneveld, Phys. Rev. A **41**, 1435 (1990).
32. P.D. Fainstein, V.H. Ponce, R.D. Rivarola, J. Phys. B **24**, 3091 (1991).
33. K. Kroneberger, A. Clouvas, G. Schüssler, P. Koschar, J. Kemmler, H. Rothard, C. Biedermann, O. Heil, M. Burhard, K.O. Groeneveld, Nucl. Instrum. Meth. Phys. Res. B **29**, 621 (1988).
34. M. Jung, thèse de l'université de Caen, 1997.
35. H. Rothard, Nucl. Instrum. Meth. Phys. Res. B **146**, 1 (1998).
36. B. Gervais, S. Bouffard, Nucl. Instrum. Meth. Phys. Res. B **88**, 355 (1994).
37. M. Jung, H. Rothard, B. Gervais, J.P. Grandin, A. Clouvas, R. Wünsch, Phys. Rev. A **54**, 4153 (1996).
38. H. Kanter, Phys. Rev. **121**, 677 (1961).
39. J.F. Ziegler, J.P. Biersack, U. Littmark, The Stopping and Ranges of Ions in Solids, *The Stopping and Ranges of Ions in Matter* (Pergamon Press, New York, 1985).
40. N. Sakamoto, N. Ogawa, N. Shiomi-Tsuda, Nucl. Instrum. Meth. Phys. Res. B **115**, 84 (1996); ICRU Rep. **49**, 111 (1993).